J Musculoskel Neuron Interact 2004; 4(4):436-441

Original Article

Hylonome

Adjusting for the partial volume effect in cortical bone analyses of pQCT images

J. Rittweger[1], I. Michaelis[2], M. Giehl[2], P. Wüsecke[3], D. Felsenberg[2]

[1]Bone Metabolism Unit, Institute for Biophysical and Clinical Research into Human Movement, Manchester Metropolitan University, Alsager, Cheshire, UK, [2]Centre for Muscle and Bone Research, Charite Campus Benjamin Franklin, Berlin, Germany, [3]Stratec Medizintechnik, Pforzheim, Germany

Abstract

Quantitative analyses of computed tomography images are prone to errors due to the partial volume effect which affects objects (e.g., bones) that have a different size or are assessed with different resolution. We have developed a set of equations suitable for both modeling the partial volume effect in cortical bone and for performing the corresponding adjustment. Seven hollow cylinders and 2 cuboid phantoms were made out of Al with 1% Si. The specimens were scanned with a pQCT machine (XCT2002, Stratec Medizintechnik, Pforzheim, Germany) and analyzed with the integrated software, version 5.50. Measurements were performed at different resolutions (voxel size = 0.20 to 0.75 mm), both in air and in Ringer solution, and analyses were performed at different detection thresholds. Applying the correcting equations set we could reduce the errors in cortical density by about 80%. The cortical area was assessed with a negligible error at a threshold (θ_0) that is equivalent to the mean of the cortical bone density and of the background density. On chosing θ_0 as the detection threshold the error in density was lowered to less than 2%. We propose to assess cortical area and cortical density in several steps, first assessing the area and density thereafter. Applying this method should be beneficial whenever 'true world' values are required, or objects of different size are compared.

Keywords: Bone Geometry, Image Analysis, Software Algorithm, Bone Scan, Cross-sectional Analysis, pQCT, Error Correction, Bone Absorptiometry, Bone Density

Introduction

Quantitative measurements of bone mass and architecture have increased our knowledge about many physiological and clinical conditions[1,2]. In the past years, peripheral Quantitative Computed Tomography (pQCT) has been developed as a highly reliable method to obtain and analyze bone scans[3] and has consequently been applied in numerous studies. Bone densities of pre- and postmenopausal women[4], of athletes and sedentary subjects[5] and values for children at different ages have been compared[6,7]. In all these reports, cortical density (ϱ), cortical cross-sectional area (A_{CRT}), and the periosteal or endocortical circumferences have been found to differ, and physiological and pathophysiological inferences have been made accordingly. These inferences, however, might partly be corroborated by the so-called 'partial volume' effect. In growing children, for instance, cortical density increases, but so does the cortical area. Unfortunately, the latter two variables are both affected by the partial volume effect. Thus, for example, a child with a comparatively thin cortical bone shell, based on an erroneously low cortical density might be misdiagnosed as a patient with osteomalacia. Hence, it would be desirable to account for such errors.

The partial volume effect emerges from projecting a continuous object on a discrete grid8,9. Hence, quantitative image analysis is prone to errors where the edge of the object is comprised inside the sampling grid. The same happens when ACRT is estimated by threshold detection algorithms: the estimation of ACRT depends on the detection threshold

P. Wüsecke is an employee of Stratec Medizintechnik.

Corresponding author: Jörn Rittweger, Bone Metabolism Unit, Institute for Biophysical and Clinical Research into Human Movement, Manchester Metropolitan University, Alsager, Cheshire, ST7 2QL, UK
E-mail: j.rittweger@mmu.ac.uk

Accepted 17 June 2004

Abbreviations

	Variable	Unit	
ϱ	X-ray determined density	[kg m^{-3}]	CRT_DEN
ϱ_A	ϱ of the area A	[kg m^{-3}]	
ϱ_B	ϱ of the background	[kg m^{-3}]	
ϱ_{Vox}	ϱ of a given voxel	[kg m^{-3}]	
A	true cross-sectional area of the figure	[m^2]	
λ	circumference length of A	[m]	PERI_N + ENDO_N
Θ	detection threshold	[kg m^{-3}]	THRESHCRT
Θ_{Rel}	Relative detection threshold. A value of 1 means $\Theta = \varrho$ of the figure, and a value of 0 means $\Theta = \varrho$ of the background (for exact definition see Equation A.6 in the Appendix)		
A_0	cross-sectional area where $\varrho_{Vox} = \varrho_A$	[m^2]	
θ_0	threshold where $A = A_{(\theta)}$	[kg m^{-3}]	
$A_{(\theta)}$	detected cross-sectional area, as defined by $\theta < \varrho_{Vox}$	[m^2]	CRT_A
H	true halo area, as defined by $\varrho_A > \varrho_{Vox} > \varrho_B$	[m^2]	
$H_{(\theta)}$	assessed halo area, as defined by $\varrho_A > \theta > \varrho_{Vox}$	[m^2]	
s	edge length within a voxel; $s << \lambda$	[m]	VOXEL SIZE

(θ) chosen. In fact, ACRT(θ) increases as the threshold decreases*. Likewise, the estimation of the periosteal circumference yields smaller, and that of the endocortical circumference greater values at higher thresholds. The estimation of ϱ is exposed to errors from either or both, by the estimation of A(θ) and the set of voxels selected.

The partial volume effect increases with the voxel size (i.e., at lower image resolution), and decreases with the object size. The question is how much. So, the results of studies on bones of varying dimensions employing the same voxel size may be a matter of concern. Thus, we propose a simple method for adjusting the pQCT area and density data for most of the errors derived from the partial volume effect.

Material and methods

An elaboration of the above arguments provided a set of equations which is given in the appendix. Physical measurements have been performed on specimens especially designed for testing the equations set (see the end of this article). As a material for those phantoms, Al with 1% Si was chosen, because its X-ray absorption is similar to that of solid bone tissue. The specimens were manufactured in different shapes in order to show either a circular or a square section, and were measured to the nearest 10 m. Cylindrical specimens resembled bone diaphyses, the projection of which on the image matrix should be similar at all angles of z-axis rotation. Squared ones showed only two different crossing angles between their surface and the image grid. In order to minimize beam hardening effects, all phantoms were designed with the same wall thickness.

Seven hollow cylinders were manufactured with an outer diameter (D) varying between 5 and 35 mm in 5-mm steps, and an inner diameter (d) 5 mm less than D. Two cuboids were manufactured with a base edge length of 5 mm. The length of all specimens was 50 mm.

All measurements were performed with an XCT-2002 machine (Stratec Medizintechnik, Pforzheim, Germany). The specimens were mounted on a specially designed support and positioned orthogonally in the measurement plane. Measurements were performed placing the specimens either in air or within a Ringer solution, mounted inside the lid of a plastic tube which was filled and closed avoiding generation of air bubbles.

Measurements were made at 0.2, 0.4, and 0.75-mm voxel sizes. Each determination was analyzed as the average of measurements comprising 5 images that were separated by a 2-mm distance. The cylindric specimens were measured only once under each set of conditions. The cuboid specimens were measured 6 times, repositioning the samples in each instance after rotation at an angle φ increasing from 0° to 90° in steps of 18°. In total, 45 different sets of measurements were performed.

* Since we deal here with quantitative bone analyses, we generally assume that ϱ of the detected figure is greater than ϱ in the background.

Image analyses of the CT scans were performed with the integrated XCT software in its version 5.50 (as per the provided 'loop functions'). This software separates bone and soft tissue by an attenuation threshold θ. Usually, θ is given in mg · cm^{-3}, but here it is more convenient to use θ_{Rel}, which can vary between 0 (density of the background) and 1 (density of the bone). Different attenuation thresholds θ_{Rel} were applied, ranging from 0.2 to 0.8. From the resulting database, the assessed variables 'CRT_A', 'PERI_N', 'ENDO_N', 'CRT_DEN', and 'VOXEL SIZE' were extracted as the figure's cross-sectional area A_{CRT}*, the outer and inner circumferences, the figure's material density, ϱ_A, and the image's voxel size, respectively (see Table of abbreviations). The figure's total circumference λ* was taken as 'PERI_N* + 'ENDO_N*' **. As a convention, both the theoretical and known values are represented by plain characters (A_{CRT}, λ, ϱ_A). Theoretical values that depend on the detection threshold θ are denoted as functions of θ ($A_{CRT}(\theta)$, $\lambda(\theta)$, $\varrho_A(\theta)$). Values obtained from physical measurements and the subsequent threshold detection are marked with an asterisk (A_{CRT}*, λ*, ϱ_A*). Values corrected by equation A.12 and A.13 are marked '^' (A_{CRT}^, ϱ_A^).

Material density was determined by defining appropriate regions of interest (ROIs), containing no part of the halo area H (Figure 2), with the software option 'density'. The relative errors made by the XCT detection algorithm were computed as the differences between the measured and known values, divided by the known value, expressed as a percentage, as

$$Err^*_x = 100 \cdot \frac{X^*-X}{X}$$

where X is one of the variables A_{CRT}, 'ENDO_N', 'PERI_N', λ, or ϱ_A. Likewise, Err^$_X$ was computed as the error after correction, applying the formulas given in the Appendix and the known values for the independent variables.

Statistical analyses were performed with the SPSS software in its version 10.0 (SPSS Inc., Chicago, USA).

Results

The bone material density ϱ_A was 1619.2 mg·cm^{-3}, the density of the Ringer solution (ϱ_B) being 66.4 mg·cm^{-3}. Air density has been theoretically regarded as ϱ_B = -303.0 mg·cm^{-3}. This 'negative' density value arises from the calibration convention of the XCT software, where fat tissue is assumed to have a density of 0. Hence, the expected 'central' threshold θ_0 was calculated as 842.8 mg·cm^{-3} for the measurements in Ringer solution and 658.1 mg·cm^{-3} for those made in air.

Adjusting the cross-sectional area A

Figure 1a gives the errors of the measured and the adjusted A_{CRT} for one hollow cylinder in Ringer solution. The

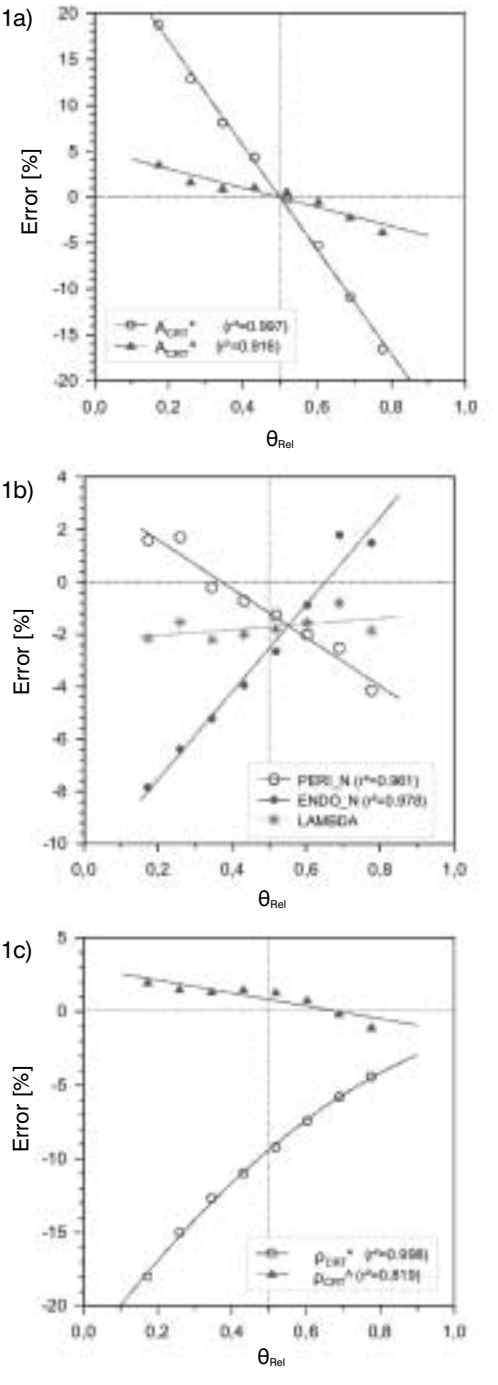

Figure 1. Errors of measured and adjusted values for the hollow cylinder with D = 15 mm and d = 10 mm in Ringer solution, given in % of the known values and plotted against the detection threshold, given in relative density values (0= ϱ_B, 1= ϱ_A, see Equation A.6).
a) Errors of the measured (open circles) and adjusted (triangles) values of cortical area A_{CRT} vary linearly with the detection threshold. They are getting close to 0 at θ_{Rel}= 0.5.
b) Errors of the measured circumferential variables: PERI_N and ENDO_N (outer and inner circumference) vary with the detection threshold. Their relationship is inverse, and hence their sum (λ) is close to constant (no significant correlation).
c) Errors of the measured (open circles) and adjusted (triangles) values of ϱ_A. For the measured value, the values were fitted to a 2nd order polynomium.

** PERI_N and ENDO_N are not included in the standard version 5.50, but an upgrade is available from the manufacturer.

	over thresholds Θ_{Rel} 0.1-0.9		Θ_{Rel} = 0.5	
	measured	**adjusted**	**measured**	**adjusted**
A_{CRT}	11.8 (4.27)	2.35 (0.86) ***	1.06 (0.69)	1.16 (1.09)
ϱ_A	9.81	1.90 (0.99) ***	9.05 (4.76)	1.57 (1.03) ***

Table 1. Absolute errors of the measured and the adjusted values for A_{CRT} and ϱ_A, averaged over all 45 definition sets. *** denotes a significant difference between measured and adjusted values (Wilcoxon test, $p < 0.001$). Over all detection thresholds (left part of the table), the adjustment yielded a significant error reduction. For the detection threshold set to θ_0 (right half), only the assessment of ϱ_A was improved by adjustment.

errors of the measured values vary linearly with the detection threshold. Similar linear relationships were also observed in all other measurements showing always R^2 values greater than 0.95, thus validating equation A.12. As expected from equations A.4 and A.11, the errors are close to 0 if the detection threshold is close to θ_0, i.e. $\theta_{Rel} \sim 0.5$.

As shown in Figure 1a, the error in $A_{CRT}\hat{}$ is considerably smaller than than in A_{CRT}*. This improvement obtained by adjusting with equation A.12 is further evident in Table 1, where the mean absolute error in A_{CRT}*, averaged through the threshold range, is significantly greater than that in $A_{CRT}\hat{}$. Furthermore, Table 1 shows no significant error reduction for $\theta_{Rel} = 0.5$.

The estimation of the outer and inner surface length depends on the detection threshold (Figure 1b). At increasing thresholds, the measured outer perimeter increases while the measured inner perimeter decreases. Those linear relationships were highly significant in all the hollow cylinders measured whereas the error of the total perimeter length λ showed relatively constant values.

Adjusting density

Figure 1c depicts the errors of measured and adjusted ϱ_A values for the same hollow cylinder as in Figure 1a and 1b. The errors of the measured values depend non-linearly on the detection threshold. In all measurements, a second order polynomial fit yielded an $r^2 > 0.98$.

The error in estimating ϱ_A decreased after correction following Equation A.13 (Table 1) and the absolute error decreased significantly by appropriate adjustment. As for the adjustment of A_{CRT}, this was true over all the threshold range, but especially for the adjustment at the detection threshold θ_0.

Discussion

These results demonstrate that the adjustment of the measured cross-sectional area A_{CRT} as per Equation A.12 and object density ϱ_A according to Equation A.13 can correct for about 80% of the partial volume effect in our specimens (Figure 1). With specimens of dimensions similar to children's or small animals' bones, the errors in assessing ϱ_A were as great as 10%. This observation underlines the importance of adjusting for the partial volume effect when assessing cortical density.

No significant improvement, however, was obtained for the assessment of A_{CRT} if the detection is performed at threshold θ_0. As a matter of fact, θ_0 itself is dependent on ϱ_A (Equation A.11), which in turn is as unknown *a priori* as A_{CRT} is.

Given the validity of the applied equations, the error in A_{CRT}* related to the partial volume effect can be calculated (in %) as

$$E_A = 100 \cdot \frac{H}{A} \cdot \left(\frac{1}{2} - \Theta_{Rel}\right) \qquad \text{(D.1)}$$

where $H = 2 \cdot s \cdot \lambda$. As stated in the Appendix and validated by our results (Table 1, right side), E_A is 0 if the threshold is set to θ_0, thus $\theta_{Rel} = 0.5$. But what if the actual ϱ_A is different from the value used to calculate θ_0 (Equation A.11)? As an example, over-estimation of ϱ_A by 10% results in a miss-setting of θ_0 by +5% (ϱ_0 close to 0). In a typical situation, for example an ulna with $A_{CRT} = 120$ mm², $\lambda = 80$ mm, and $s = 0.6$ mm, the value of H is 96 mm², hence $E_A \sim 4\%$. Therefore, errors in the assumption of ϱ_A result in errors of A_{CRT}* that are less than half the *a priori* error.

Another point of discussion arises if ϱ_B is different at the outer and the inner background. Usually we find a ϱ_B of about 60 mg · cm^{-3} for the tissue surrounding cortical bone. The density of the bone marrow is usually slightly lower, depending on the different factors like fat content. We found values between 40 and 60 mg · cm^{-3}. These variations are small in relation to cortical bone density (< 2%). Hence, the problem seems to be negligible concerning the estimation of A_{CRT} at an accuracy of 1%.

The question now arises, how to assess A_{CRT} and ϱ_A in practice. It is clear from this discussion that the estimations of both factors are interdependent. Unfortunately, the iterative approach, adjusting A_{CRT} with an *a priori* assumed ϱ_A as a first step, next adjusting ϱ_A with the results of the former step, and so forth, will not converge. If, for example, A_{CRT} is increased at the step n, ϱ_A and θ_0 may have to be decreased at the step n+1, leading to a further increase of A_{CRT}, and so forth.

We therefore propose the following procedure:

1. Measure ϱ_B, or assume it to be 60 mg · cm^{-3} for measurement *in vivo* or entire limbs, or -300 mg · cm^{-3} for measurements of bones in air.
2. Assume some given cortical bone density value, e.g., 1360 mg · cm^{-3}.
3. Assess A_{CRT} at θ_0, e.g. at 710 mg · cm^{-3} in entire limbs or 530 mg · cm^{-3} for measurements in air.
4. Correct ϱ_A by application of Equation A.13.
5. Correct A_{CRT}, either by selecting a new detection threshold or after equation D.1

Interestingly, one of the most important conclusions from these elaborations is that adjustment of the partial volume effect may not always be necessary. It should be beneficial if

absolute instead of relative values are required, or when bones with a different λ/A ratio are compared. We think that the algorithm outlined here, though leaving some uncertainty unsolved, may be useful in these cases.

Acknowledgments

The authors are particularly grateful to Mr. Breuer and Mr. Forster for manufacturing the standard cylinders. Last but not least the authors wish to express their respect for M. Callas, who contributed a powerful stimulation for performing the Appendix.

Appendix

Basic equations

A is the area of a figure which has been processed as a digital image within a background B. Voxels of A and B are discernible by a property ϱ that scales linearly. For example, ϱ may be thought of as density. By definition, $\varrho_B < \varrho_A$.

H is the 'halo' area around the figure which is caused by 'smearing' of A's edge due to the partial volume effect. As a consequence, $\varrho_B < \varrho H < \varrho_A$. Moreover, a voxel's ϱ in H increases with the degree of overlapping with A, i.e., ϱ of a single voxel (ϱPix) in H increases with the vicinity to A.

It is further assumed that the figure sections the image voxels randomly, i.e., that within H, ϱPix is equally distributed between ϱ_A and ϱ_B. As a consequence

$$\varrho_H = \frac{\varrho_A + \varrho_B}{2} \qquad \text{(A. 3)}$$

Let A_0 be that part of the figure and B0 that of the background which is not affected by H, i.e., with $\varrho Pix = \varrho_A$ and $\varrho Pix = \varrho_B$, respectively (see Figure 1). It is obvious then that

$$A + B = A_0 + H + B_0 \qquad \text{(A. 2)}$$

Given the conservation of mass, we obtain

$$A \cdot \varrho_A + B \cdot \varrho_B = A_0 \cdot \varrho_A + H \cdot \varrho_H + B_0 \cdot \varrho_B \qquad \text{(A. 3)}$$

If the edge of the figure cuts the voxels affected by the border randomly:

$$A = A_0 + \frac{H}{2} \qquad \text{(A. 4)}$$

Now, area $A_{(\theta)}$ is assessed by a threshold detection algorithm, that assigns all voxels with $\varrho Pix > \theta$ to $A_{(\theta)}$ (Figure 2). Hence, $A_{(\theta)}$ may be thought of as composed by an area with voxels of density ϱ_A (A_0), which is not dependent of θ, and the over-threshold halo area $H_{(\theta)}$

$$A(\theta) = A_0 + H(\theta) \qquad \text{(A. 5)}$$

Let us consider the size of $H_{(\theta)}$. By definition, $\varrho_B < \theta < \varrho_A$. If θ is close to ϱ_A, the number of $H_{(\theta)}$ voxels is small. On the other hand, if θ is close to ϱ_B, $H_{(\theta)}$ is close to H.

More precisely, defining the relative threshold θRel as

$$\theta_{Rel} = \frac{\theta - \varrho_B}{\varrho_A - \varrho_B} \qquad \text{(A. 6)}$$

H(θ) turns out to be:

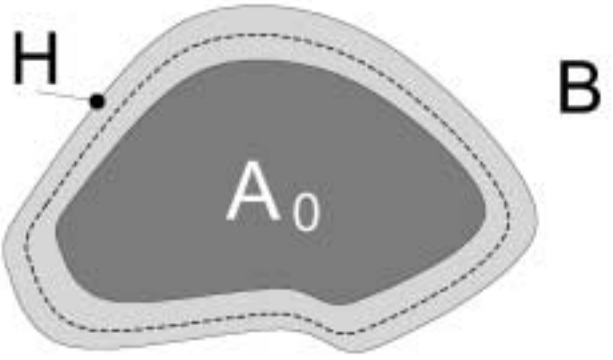

Figure 2. Figure A (marked by the dashed line) before background B appears to have a 'halo' H because of the partial volume effect, which reduces the area of A showing the 'true' density to A_o.

$$H(\theta) = H \cdot (1 - \theta_{Rel}) \qquad \text{(A. 7)}$$

Next we have to consider the circumference length λ. We expect that A is a closed area with λ » voxel edge length s. Since ϱ is conservative, i.e., because mass 'missing' in one voxel of H must appear in a neighbour voxel, we obtain

$$H = 2 \cdot s \cdot \lambda \qquad \text{(A. 8)}$$

Finally, similar to equation A.1, it follows that

$$\varrho_{H(\theta)} = \frac{\varrho_A + \theta}{2} \qquad \text{(A. 9)}$$

Applying the principle of conservation of mass to Equation A.5, we obtain

$$A(\theta) \cdot \varrho_{A(\theta)} = A_0 \cdot \varrho_A + H(\theta) \cdot \varrho_{H(\theta)} \qquad \text{(A. 10)}$$

Correcting A

Equations A.4 and A.5 imply that $A_{(\theta)} = A$ if $H_{(\theta)} = H/2$. Given that all voxels in H have a density between θ and ϱ_A and are equally distributed between these values, and solving equation A.7 we obtain the threshold θ_0 that estimates A correctly as

$$\theta_0 = \frac{\varrho_A + \varrho_\beta}{2} \qquad \text{(A. 11)}$$

In reality, ϱ_A and ϱ_B may not be known. In order to estimate A for $\theta \neq \theta_0$, we apply Equations A.4, A.5, A.6, and A.7 to obtain

$$A = A(\theta) + H \cdot (\theta_{Rel} - \frac{1}{2}) = A(\theta) + 2 \cdot s \cdot \lambda \cdot (\theta_{Rel} - \frac{1}{2}) \qquad \text{(A. 12)}$$

Correcting ϱ_A

Equation A.7 shows that $H_{(\theta)}$ is inversely related to θ, which inversely affects the estimation of $\varrho A_{(\theta)}$. On the other

hand, $\varrho_A(\theta)$ increases linearly with θ. Let us consider the error made in estimating $\varrho_A(\theta)$ more precisely. Be mA the mass in area A, and R the error in mass estimation.

$$m_A = m_{A(\theta)} + R \Leftrightarrow A \cdot \varrho_A = A(\theta) \cdot \varrho_{A(\theta)} + R$$

Substitution by Equations A.10, A.7, A.9 and A.4 yields

$$R = \frac{H}{2} \cdot \left(\frac{\theta^2 - \varrho_A \varrho_B}{\varrho_A - \varrho_B} \right)$$

Now, the equation

$$A \cdot \varrho_A = A(\theta) \cdot \varrho_{A(\theta)} + \frac{H}{2} \cdot \left(\frac{\theta^2 - \varrho_A \varrho_B}{\varrho_A - \varrho_B} \right)$$

can be solved for ϱ_A, which yields

$$\varrho_A = \frac{u + \sqrt{u^2 + 8A \cdot (H\theta^2 - 2 m_{A(\theta)} \cdot \varrho_B)}}{4A} \qquad \text{(A. 13)}$$

where

$$m_{A(\theta)} = A(\theta) \cdot \varrho_{A(\theta)} \; ; \; u = (2A - H)\varrho_B + 2 m_{A(\theta)}$$

References

1. Schiessl H, Frost HM, Jee WS. Estrogen and bone-muscle strength and mass relationships [see comments]. Bone 1998; 22:1-6.
2. Liberman UA, Weiss SR, Broll J, Minne HW, Quan H, Bell NH, Rodriguez-Portales J, Downs RW, Jr, Dequeker J, Favus M. Effect of oral alendronate on bone mineral density and the incidence of fractures in postmenopausal osteoporosis. The Alendronate Phase III Osteoporosis Treatment Study Group. N Engl J Med 1995; 333:1437-1443.
3. Sievanen H, Koskue V, Rauhio A, Kannus P, Heinonen A, Vuori I. Peripheral quantitative computed tomography in human long bones: evaluation of *in vitro* and *in vivo* precision. J Bone Miner Res 1998; 13:871-882.
4. Ferretti JL, Capozza RF, Cointry GR, Schneider P, Reimers C, Schiessl H. Bone mass is higher in women than in men per unit of muscle mass but bone mechanostat would compensate for the difference in the species. Bone 1998; (Suppl.5):S471.
5. Rittweger J, Beller G, Ehrig J, Jung C, Koch U, Ramolla J, Schmidt F, Newitt D, Majumdar S, Schiessl H, Felsenberg D. Bone-muscle strength indices for the human lower leg. Bone 2000; 27:319-326.
6. Neu CM, Manz F, Rauch F, Merkel A, Schoenau E. Bone densities and bone size at the distal radius in healthy children and adolescents: a study using peripheral quantitative computed tomography. Bone 2001; 28:227-232.
7. Rauch F, Neu C, Manz F, Schoenau E. The development of metaphyseal cortex – implications for distal radius fractures during growth. J Bone Miner Res 2001; 16:1547-1555.
8. Kondo T, Ikeda T, Go J. Image processing and quantitative assessment in computer tomography for non-surgical treatment of brain tumours. Acta Neurochir (Wien) 1982; 64:19-37.
9. Prevrhal S, Engelke K, Kalender WA. Accuracy limits for the determination of cortical width and density: the influence of object size and CT imaging parameters. Phys Med Biol 1999; 44:751-764.